AMBIENT VIBRATIONS FOR MODEL VALIDATION OF A LARGE DAM: DYNAMIC STRUCTURAL BEHAVIOR

Michael Dupuis[1]
Brian Martinez[2]
Tom MacDougall[3]
Josh Corbett[4]

(Part two of a three-part paper series)

ABSTRACT

Ambient vibration data acquired from 90 unique locations on a large dam were evaluated to investigate the dynamic behavior and system interactions of structural components. This data collection program was designed to validate the dynamic properties of an LS-DYNA model, which is being used to evaluate the dam's response to earthquake ground motions. Results of the dynamic structural analysis will be used to inform an ongoing Issue Evaluation Study by the U.S. Army Corps of Engineers. Ambient vibration data were recorded over four days during normal operating conditions without forced excitation of the structure. Eleven recording instruments—four reference instruments and seven temporary instruments—were deployed for thirteen 40-minute-long test setups. These setups included locations along the right and left embankment roadways, within the three galleries (right retaining wall, lower gallery, and upper gallery), on various parts of all five spillway piers (trunnion anchor blocks, upper landing, and pier top), within the penstock hoist motor room, and at various elevations of the elevator tower. Ambient responses were evaluated based on their spectral content, and power spectral densities were used to identify where dominant behavior occurs in the dam and its components. Interaction effects were identified by comparing resonances within the dam that manifested as split resonances, indicating coupling between the components. A systems approach was used to describe the results for the entire dam and how the individual components interact. Estimates of damping showed the greatest damping in the portions of the concrete dam adjacent to the embankments and the lowest damping at the interior piers. The results indicate that the dam is a highly coupled complex system with significant interactions between various components, which are expected to influence the seismic response of the structure.

INTRODUCTION

The Risk Management Center (RMC) of the United States Army Corps of Engineers (USACE) is conducting Issue Evaluation Studies (IES) on multiple dams in the Willamette River Valley, located in Oregon. One of the primary components of these studies is to better characterize the potential seismic risk by conducting detailed structural

[1] Geosyntec Consultants Inc., Davis, California, michael.dupuis@geosyntec.com
[2] Geosyntec Consultants Inc., Davis, California, brian.martinez@geosyntec.com
[3] RJH Consultants Inc., Denver, Colorado, tmacdougall@rjh-consultants.com
[4] U.S. Army Corps of Engineers, Louisville, Kentucky, josh.m.corbett@usace.army.mil

analyses of the dams considering static and seismic loading. As part of these assessments, linear and nonlinear LSDYNA finite element models are being used to better understand the seismic performance of dams within the USACE IES process. Foster Dam, a rockfill earthen embankment dam with a central concrete spillway, is the first such analysis currently underway.

For certain potential failure modes of Foster Dam, the structural demands, failure thresholds, and potential damage may be sensitive to the dynamic characteristics of the structural model, in particular the modal frequencies, damping, and interactions between the various structural components. Therefore, validation and calibration of the dynamic properties in the finite element model with recorded data are necessary.

Ambient vibration data were recorded from various critical components of Foster Dam, labeled in Figure 1, which included the concrete gravity monoliths, a reinforced concrete tower, spillway piers, and adjacent embankments, including the spillway retaining walls. The ambient vibration data were analyzed to identify the dynamic characteristics of various features of the dam in support of development of finite element models and to improve understanding of the system interactions of the structural components.

This paper is part two of a series of technical papers on ambient vibration data collection (Dupuis et al, 2025), dynamic behavior and component interactions, and LS-DYNA modeling efforts (planned for USSD 2026). Part one focuses on the specifics of the testing program including instruments, test setups, and means and methods, and shares successful testing strategies and lessons learned (Dupuis et al, 2025). Part three will apply the estimated dynamic properties to validate an LS-DYNA model of Foster Dam.

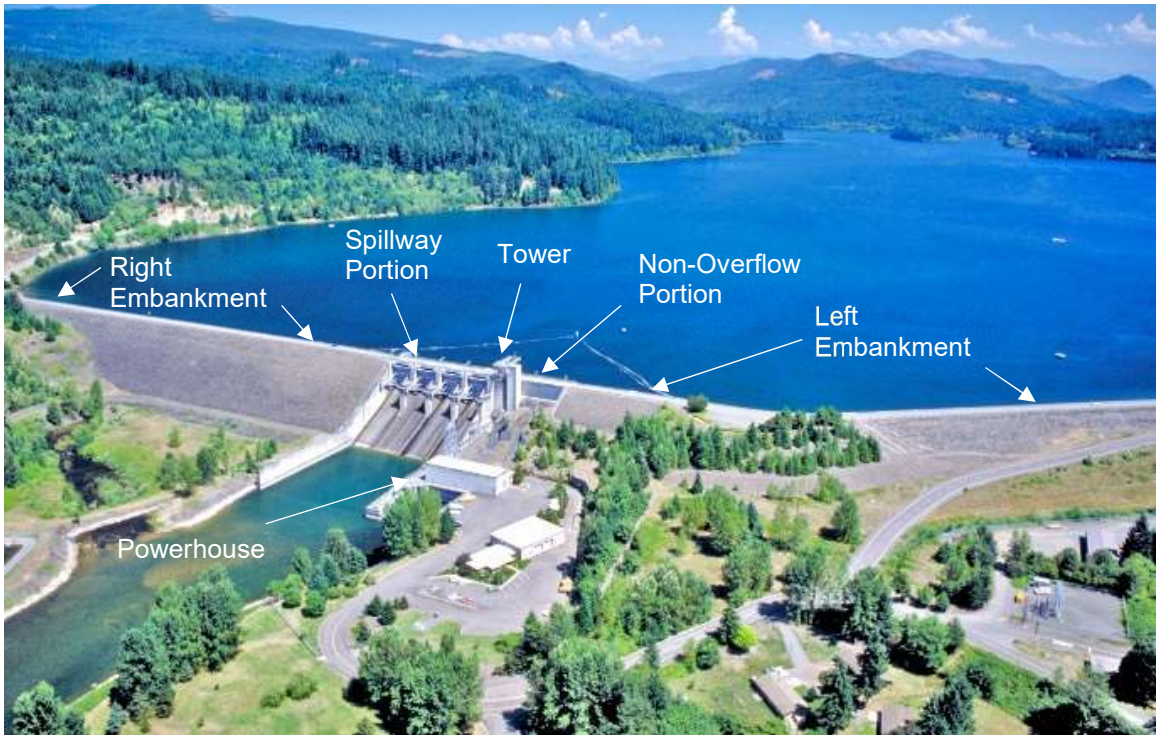

Figure 1. Aerial view of Foster Dam (Recreation, 2024).

DATA SUMMARY AND BACKGROUND

Instrumentation and Testing

The data were recorded over four days during close to normal operating conditions and without intentional forced excitation of the structure. Eleven recording instruments (four reference instruments and seven temporary instruments) were deployed for thirteen 40-minute-long test setups (TS) and two stand-alone deployments (SD) in the elevator tower and on bedrock. The specifics of the instrumentation and testing program are presented in detail by Dupuis et al (2025).

Ambient responses were acquired using accelerometers with full scale range of 2 g and with self-noise of 20 μg/√Hz (Sensequake, 2023) and velocimeters with 120 mm/s full-scale range and with 10^{-2} μg/√Hz self-noise from 1 to 20 Hz (Sensequake, 2023). Data quality was assessed based on a review of the time and spectral characteristics. The recorded vibrations include both steady-state ambient noise and transient events.

Transient Events and Steady-State Data

For test setups recorded while the crest road was open, transient events, such as those apparent in Figure 2, were introduced by vehicles as they moved longitudinally along the axis of the dam; therefore, the timing of the peak accelerations differs at different instrument locations. A trimmed duration of 15 seconds was found to be sufficient to encompass transient vibrations at all sensors for each event. Seven transient events were selected from each test setup and stand-alone deployment. Instances where multiple vehicles caused closely spaced transients, visible in the time domain as overlapping wave trains, were not selected.

TS-8, TS-9, TS-10, TS-A, and SD-Bedrock did not contain transient events because they were recorded while the crest roadway was closed or were recorded from downstream bedrock well separated from the roadway (Dupuis et al, 2025). Low-amplitude steady-state ambient vibrations along the right embankment during TS-8 are shown in Figure 3.

To facilitate different methods of analysis, which can variously make use of steady-state and transient data, windows of each type of behavior were extracted from each test setup and stand-alone deployment. The acceleration data is judged to be best suited for the relatively high-amplitude transient events, which exhibit up to 0.2 g during the onset of vehicle-induced transients. The velocity data is judged to be best suited for steady-state recordings (i.e., data recorded during road closure) for which ambient acceleration levels range from 1 to 5 mg.

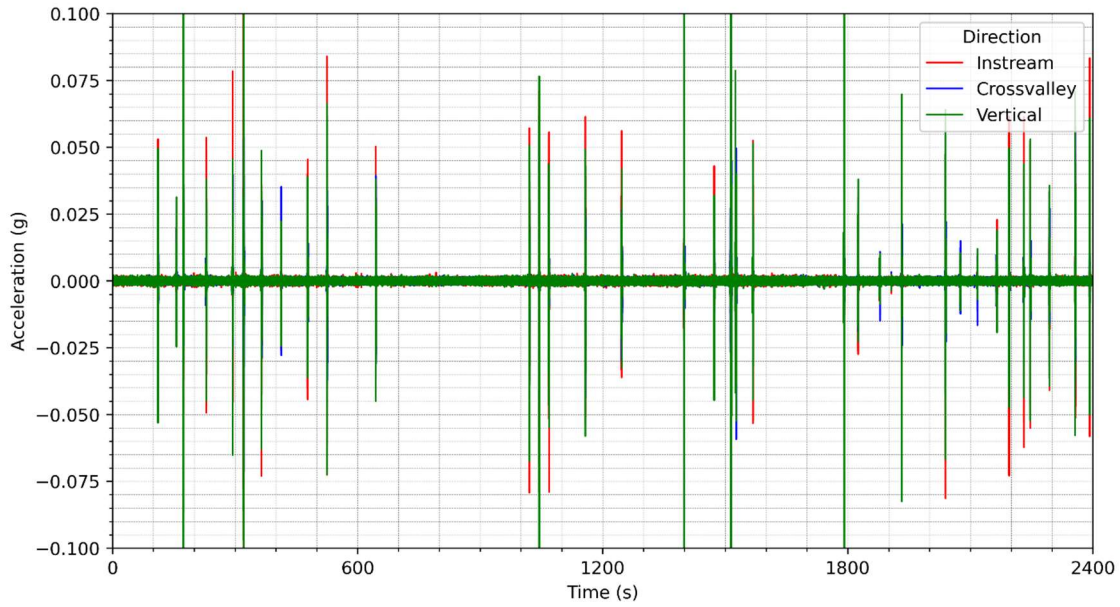

Figure 2. Transient events: ambient response acceleration time series data collected from Tower — Top Level (TS-6, Instrument 1) while the crest road was open.

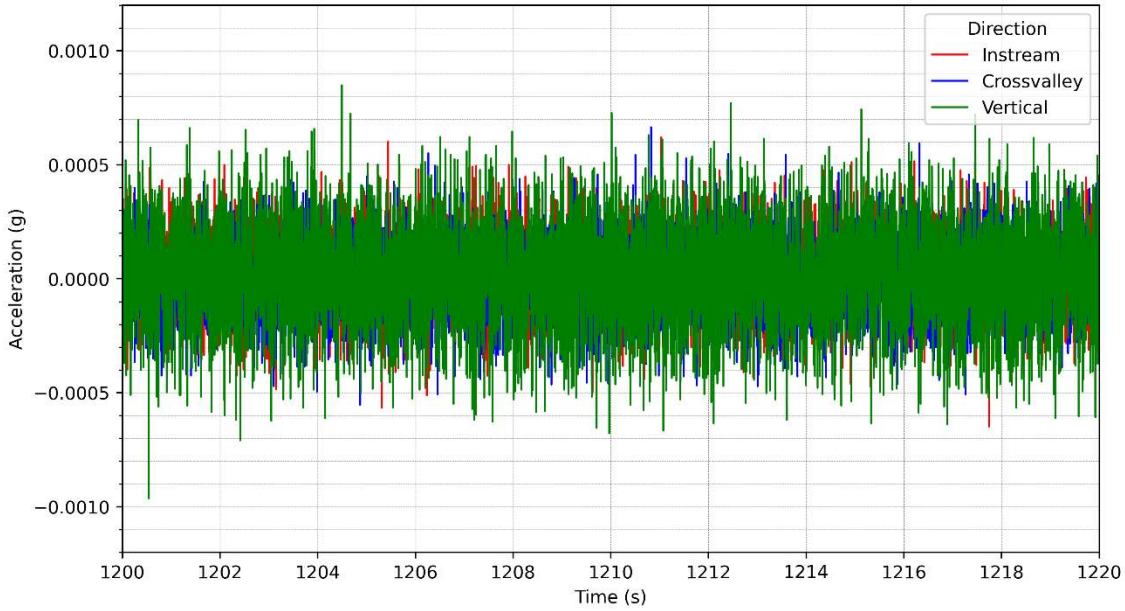

Figure 3. Steady-state data: ambient response acceleration time series data collected from the Right Embankment — Station 21+70.0 (TS-8, Instrument 4) during the crest road closure.

Data Pre-Processing

The following pre-processing steps were applied to all full-length acceleration and velocity time series:

1. Load either acceleration data (for transient events) or velocity data (for steady-states) from the human-readable text files. For velocity data, numerical differentiation was performed to estimate associated accelerations;
2. Scaled records from units of m/s^2 to g;
3. The 15-s time series for each transient event was trimmed and extracted as an independent time series, as shown in Figure 4. Similarly, the steady-state portions were segmented into 15-s-long time series and were extracted as independent time series;
4. Linear detrend and removal of mean offset for each segmented time series;
5. The segmented 15-s-long time series were set to have start times of 0 s;
6. A Tukey (tapered cosine) window was applied to each segmented time series with 10% of the duration within each tapered region at the start and end; and
7. Rotation of the horizontal components to be orthogonal with the longitudinal and transverse axis of the dam (as required); and
8. Save the pre-processed time series in .aaa format.

Identification of Powerhouse Harmonics

A stand-alone deployment with a single instrument was used to record data from bedrock from an accessible location adjacent to the powerhouse and downstream of the left embankment approximately 230 ft from the powerhouse turbines. These data were investigated to identify the presence of harmonics associated with rotating equipment from the powerhouse. Peaks in the fast Fourier transformation (FFT)-based power spectral density (PSD) in all three directions were identified at multiples of 4.285 Hz, as shown in Figure 4. These harmonics are suspected to be associated with the frequency of the generating units within the powerhouse, with a nameplate rotational speed of 257 rpm. By identifying the powerhouse harmonics from the bedrock location, which was separated from the structural components of the dam, there can be greater confidence that peaks at identical frequencies observed in spectra from other structural components are due to influences of these harmonic vibrations. These suspected powerhouse harmonic frequencies are indicated in all spectral plots with dash-dotted lines.

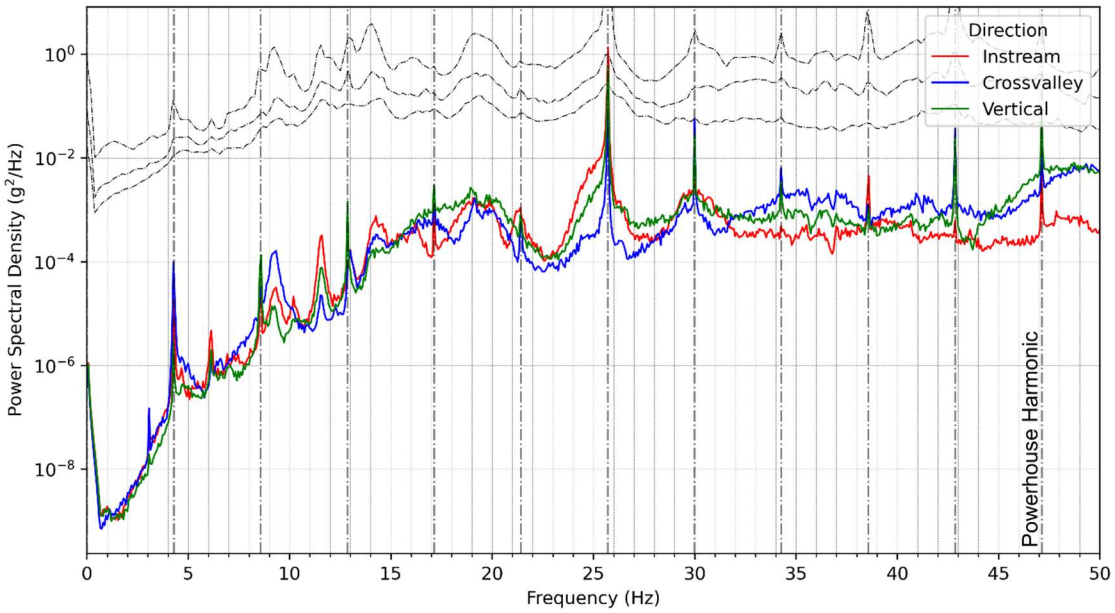

Figure 4. Bedrock recording: power spectral densities with powerhouse harmonics apparent as spectral peaks at multiples of 4.285 Hz (indicated with vertical dash-dotted lines). Dashed spectra indicate results from ARTeMIS singular value decomposition of the global dam model.

SPECTRAL ANALYSIS AND DAMPING ESTIMATION METHODS

Maximum Entropy Method

The rigid formulation of the FFT-based PSD includes amplitudes of the complex exponential that exactly reproduces the signal and noise. This results in high variability in amplitudes over relatively small changes in frequencies and makes it difficult to identify the powerful resonant behavior with which we are concerned. To address these shortcomings in the FFT-based spectra, an entropy-based technique—the Maximum Entropy Method (MEM)—was adopted for estimating PSD, and MEM-based PSD were used to identify frequencies in the structures that contain the most power.

MEM-based PSD remove the rigid mathematical constrictions of periodicity and instead rely on curve fitting to the power of the signal based on the contents of the signal (Marple, 1987). It is noted that spectral peak widths of the power spectral densities computed via the maximum entropy method are sensitive to the selected model order and therefore judgement was required to determine appropriate parameters. MEM-based PSD computed via entropy-based methods, which better account for the dominant energy of the system, are considered in the subsequent sections.

Computation of Spectral Ratios

Horizontal-to-Vertical. Horizontal-to-vertical spectral ratios (HVSR), and various geometric mean spectra thereof, were computed from the pre-processed time series. The following procedure, which is similar to that of Smith et al (2024) who analyzed earthquake-induced records at embankment dams, was applied to compute HVSR at various locations on different structural components of the concrete portion of the dam:

1. Load the pre-processed acceleration time series from .aaa format;
2. Calculate the MEM-based PSD for each channel;
3. Calculate the HVSR, for both the instream horizontal and crossvalley horizontal directions, by dividing the PSD for each horizontal channel by the corresponding PSD for the vertical channel;
4. Compute the square root of these PSD ratios; and
5. Calculate the geometric mean of the HVSR.

Structure-to-Gallery. The following procedure was applied to compute structure-to-gallery spectral ratios (SGSR) at various cross-sections for selected structural components of the dam. A single gallery location was used for each block—the gallery location within that block. Eight gallery locations were used in total, one for each concrete dam block. For Block 1 through Block 5, these were located within the lower gallery; for Block 6 through Block 8, these were located within the upper gallery. The following processing steps were applied to the pre-processed time series to compute the SGSR at all locations in the concrete portion of the dam.

1. Load the pre-processed acceleration time series from .aaa format;
2. Calculate the MEM-based PSD for each channel of each segmented transient event;
3. Calculate the SGSR by dividing the PSD for each transient event's structural channel by the corresponding PSD for each gallery channel (e.g., instream structural channels were compared to instream gallery channels within each cross-section);
4. Compute the square root of these PSD ratios; and
5. Calculate the geomean of the SGSR for each instrument of each test setup.

Damping Estimation

Estimates of first-mode damping were made using two methods: (i) the half-power bandwidth method, and (ii) the logarithmic decrement approach applied to random decrement signatures computed with a triggering threshold of $\sqrt{2}\sigma$ (Casiano, 2016). These methods were applied to the pre-processed transient event time series induced by vehicle loads band-pass filtered with a 4^{th} order Butterworth filter with low and high cut-off frequencies of 5 Hz and 20 Hz, respectively.

OBSERVED DYNAMIC STRUCTURAL BEHAVIOR

Identification of Structural Resonances

Analysis of spectral ratios provided insights into resonant behavior in various structural components. Example PSD, SGSR, and HVSR plots for the concrete spillway and right embankment portions of the dam are shown in Figure 5 through Figure 10. For reference locations, or temporary locations that were part of multiple test setups, multiple lines are shown—one for each test setup. Estimates of resonant frequencies for various structural components of interest are indicated. These estimates are summarized and presented for the concrete spillway and embankments in Figure 12 and Figure 13, respectively.

Presence of Component Interactions

Crossvalley interaction effects are observed between the piers and the tower, as shown in Figure 6 through Figure 8. Because the resonances of the various components interact, the resonant peaks for the piers in the crossvalley direction are slightly offset but occupy frequencies from 10–14 Hz. There is a suspected dead zone—a frequency band with attenuated behavior—in the tower crossvalley direction from 10–14 Hz (not shown), which is inferred from the slight trough in this range. These interaction effects may increase with stronger (e.g., earthquake) shaking; i.e., at ambient levels, the interaction effects may not be fully developed.

The interaction effects may indicate that there are relatively competent interfaces between the structural components (piers and tower). However, during very strong ground shaking, i.e., the conditions with which we are primarily interested, these interfaces may degrade or separate, at which point the interaction effects would diminish, the attenuated behavior observed in the tower may decrease, and the crossvalley resonances may shift as they no longer compete to occupy the same spectral frequencies.

ARTeMIS Modal Analysis

In a parallel analysis to the spectrum-based analysis, ARTeMIS Modal (ARTeMIS, 2023) was used to complete an operational modal analysis (OMA) which can be used to determine deflected mode shapes from ambient vibration data. Mode frequencies and shapes were estimated via the enhanced frequency domain decomposition (EFDD) method. EFDD was used to produce the frequency and mode shapes for the spillway portion of the concrete dam. ARTeMIS relies on singular value decomposition; therefore, local resonances which were identified at similar but adjacent frequencies by spectral-based methods, were combined into a single global mode and frequency.

Estimates of Damping

The damping estimates were found to be sensitive to the triggering threshold, frequency filtering, and model order. Damping estimates were highest for the concrete components adjacent to the rockfill embankments and were lowest for the interior piers.

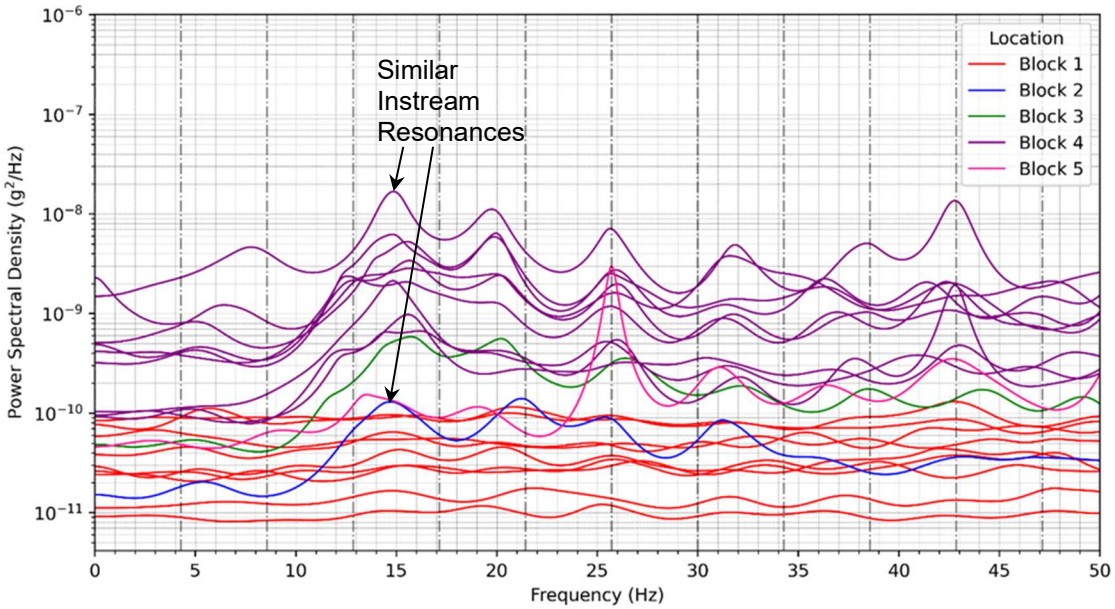

Figure 5. Power spectral densities in the instream direction at the top of the piers of Block 1 through Block 5. Multiple lines are shown for Block 1 and Block 4, which were reference locations.

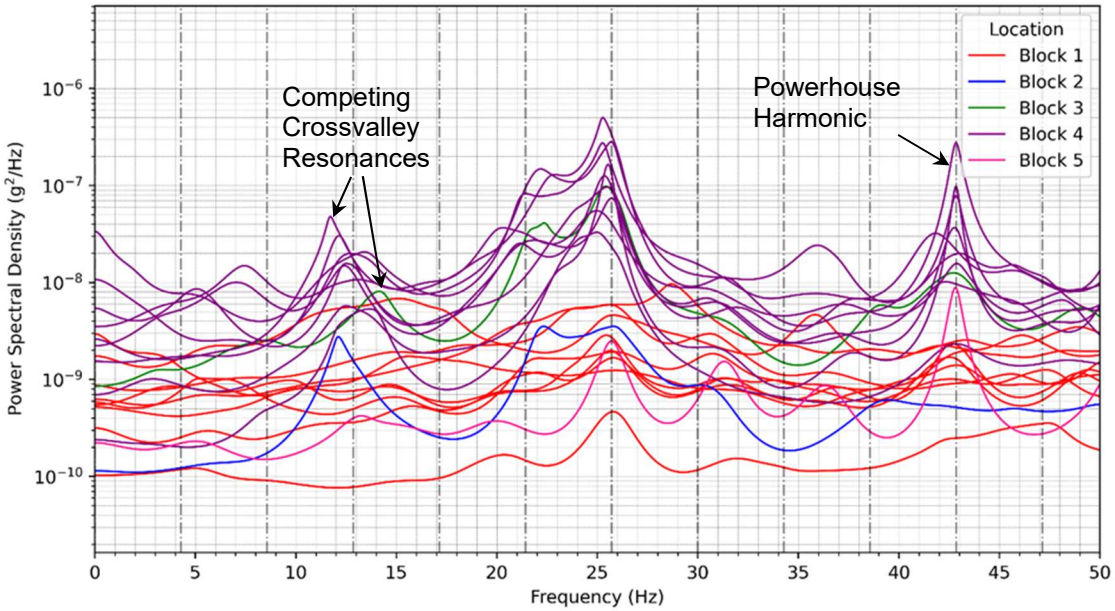

Figure 6. Power spectral densities in the crossvalley direction at the top of the piers of Block 1 through Block 5. Multiple lines are shown for Block 1 and Block 4, which were reference locations.

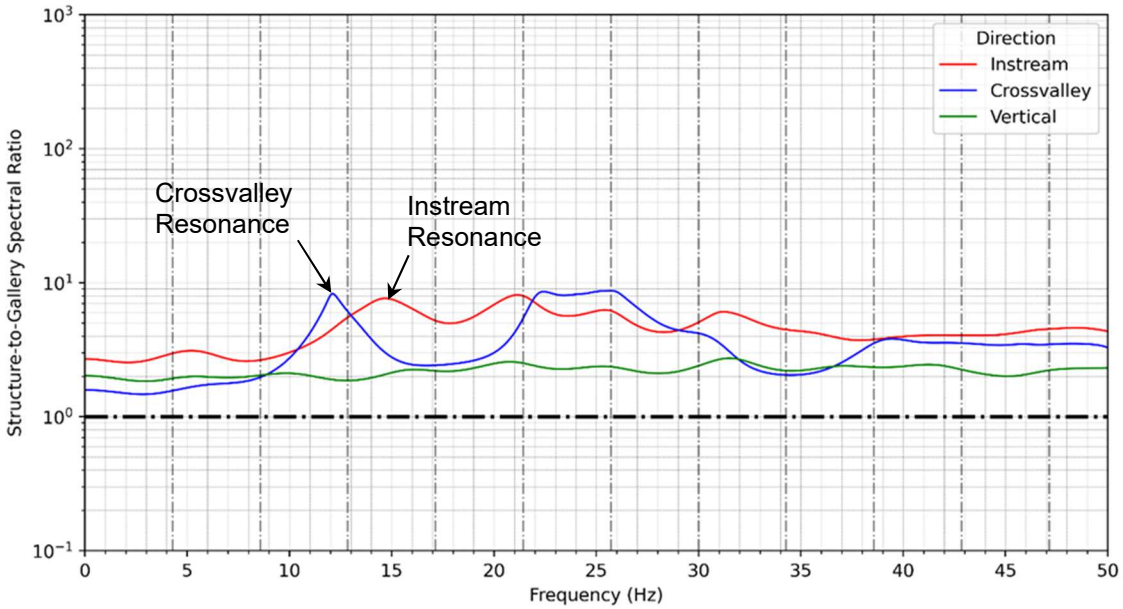

Figure 7. Block 2 — Pier Ladder Top structure-to-gallery spectral ratio (TS-2).

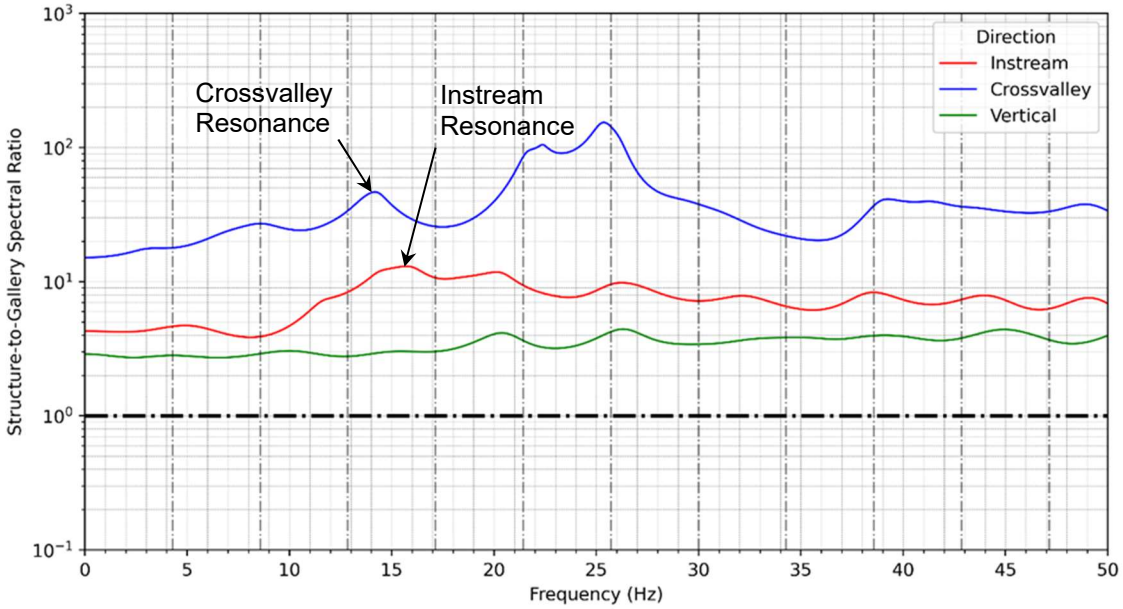

Figure 8. Block 3 — Pier Ladder Top structure-to-gallery spectral ratio (TS-3).

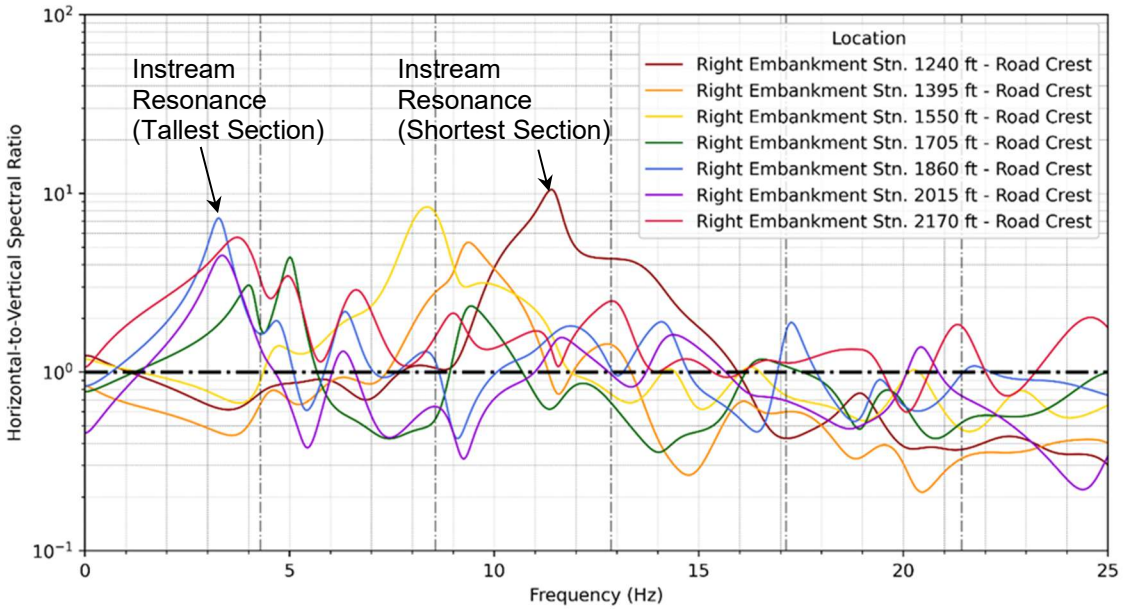

Figure 9. Right embankment roadway crest — instream horizontal-to-vertical spectral ratio (TS-8).

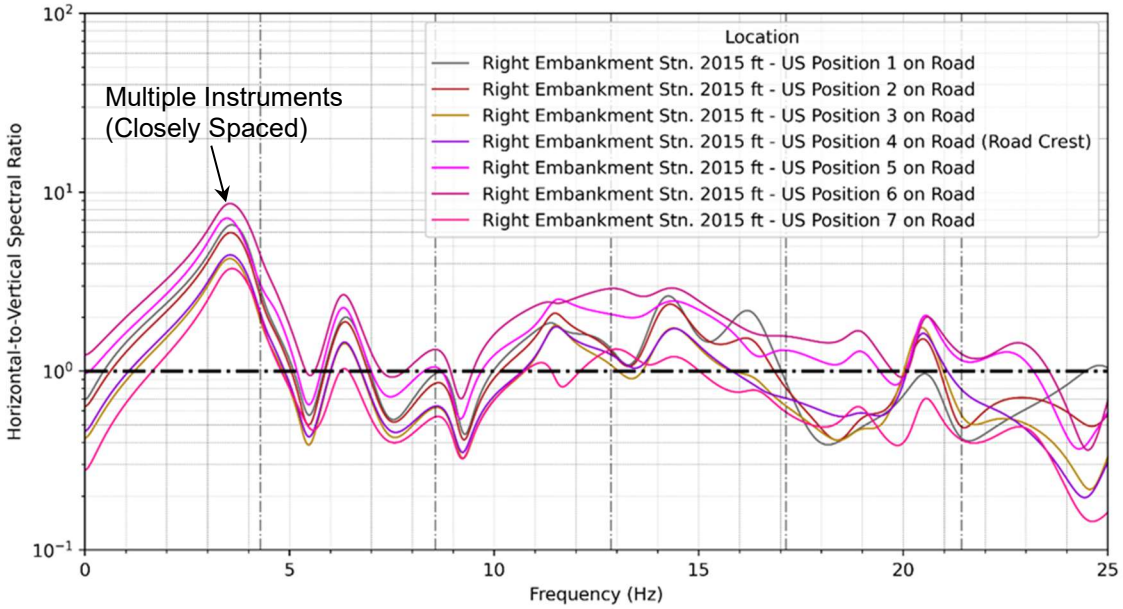

Figure 10. Right embankment at Station 20+15.0 — instream horizontal-to-vertical spectral ratio (TS-A).

COMPARISON WITH ESTIMATES FOR OTHER DAMS

To develop context for the results for Foster Dam, a literature review of damping and resonant frequencies for concrete and embankment dams by others was completed. This allowed for the estimates for Foster Dam to be compared to estimates for other dams made by other field investigations.

Estimates of modal damping for a selection of 32 concrete dams made from analysis of forced vibration acceleration data are shown in Figure 11. Figure 12 and Figure 13 compare the concrete and embankment portions of Foster Dam with estimates of dynamic behavior of these types of dams by others.

The concrete and embankment portions of Foster Dam exhibit relatively high instream resonant frequencies; however, Foster Dam is relatively short, and the frequency estimates are consistent with the trend of frequency estimates with dam height.

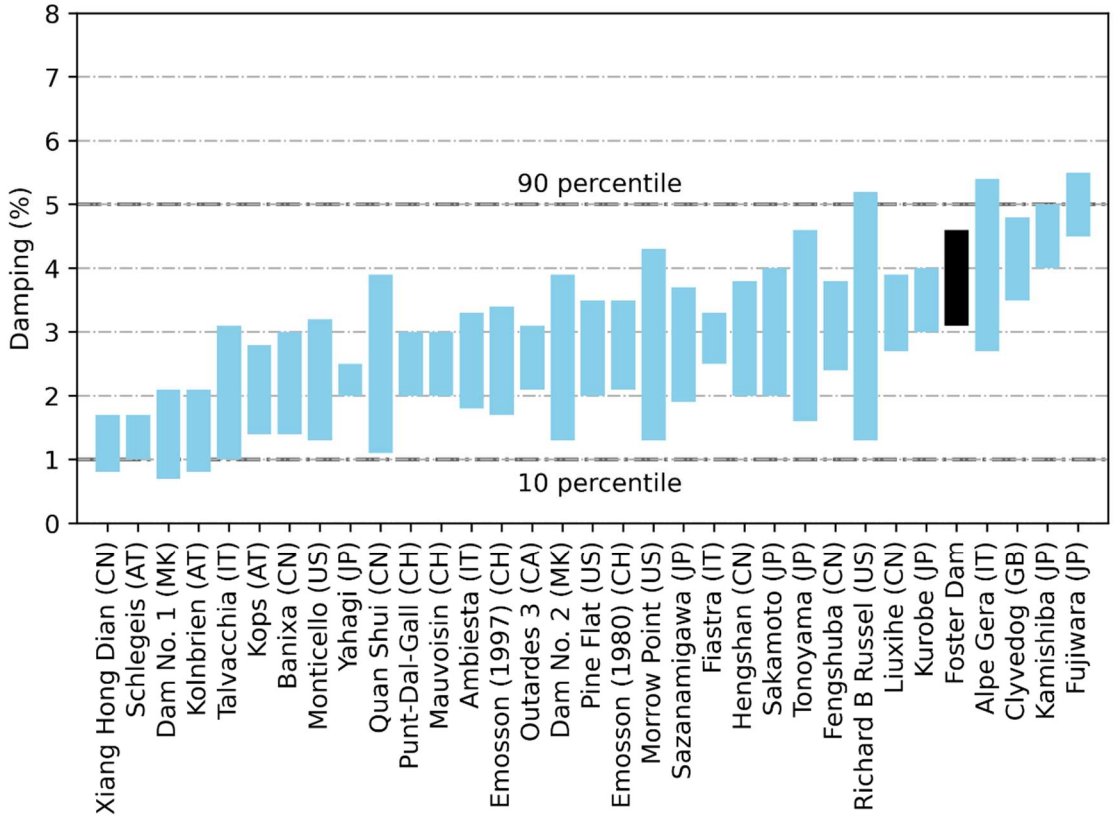

Figure 11. Estimated damping in the instream direction of the non-overflow portion of Foster Dam compared with estimates for selected concrete dams based on forced vibration measurements. The range for each dam shows the minimum and maximum damping values measured at the first five resonant frequencies (Chopra, 2020).

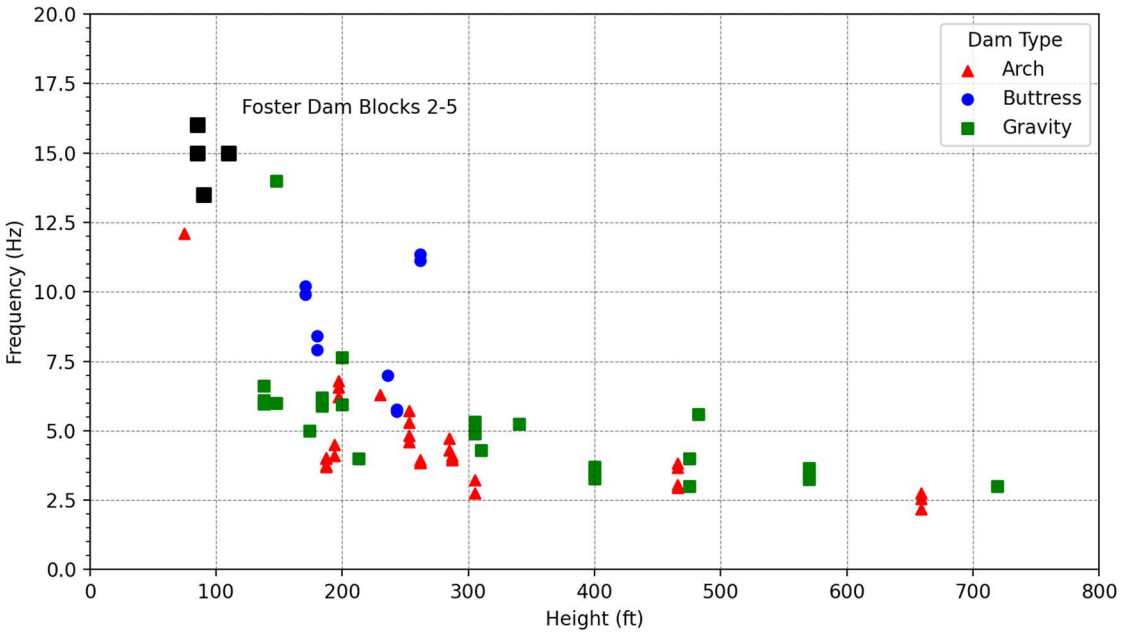

Figure 12. Instream resonant frequency estimates for the concrete spillway portion of Foster Dam compared with instream resonant frequency estimates for selected concrete dams compiled from other studies (Abdulamit et al, 2017; Calcina et al 2014; Daniell and Taylor, 1999; Duron et al, 2018; Duron 1996; Hall 1988).

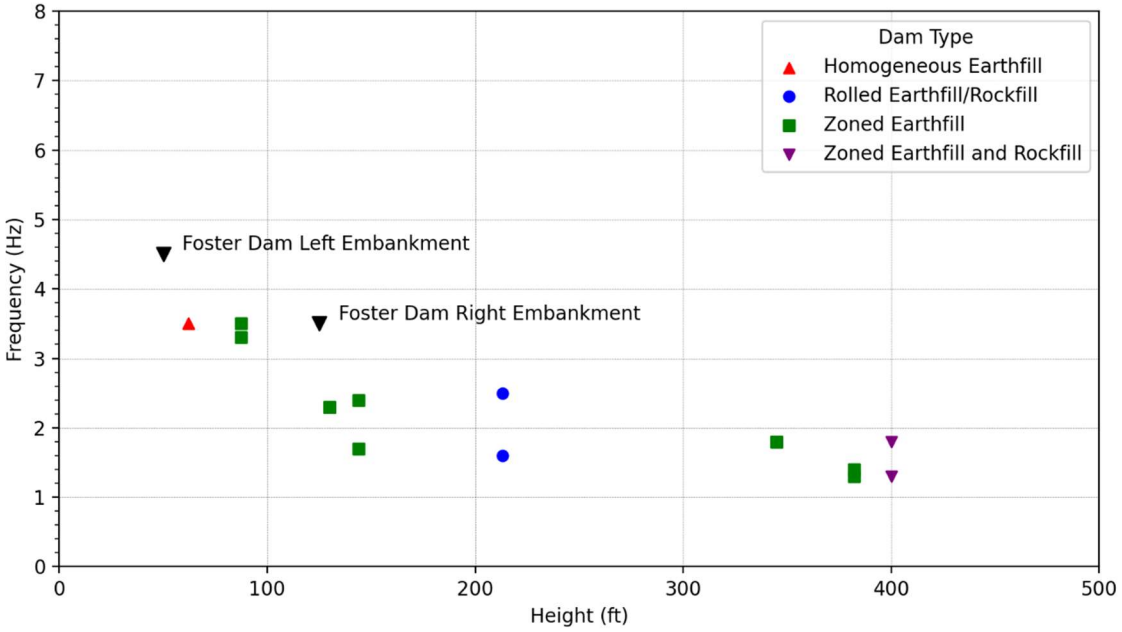

Figure 13. Instream resonant frequency estimates for the embankments of Foster Dam compared with instream resonant frequency estimates for selected earthfill and rockfill dams by Smith et al (2024).

CONCLUSION

Ambient vibration data acquired on Foster Dam were evaluated to elucidate the dynamic behavior and system interactions of the structural components. The data were recorded over four days during close to normal operating conditions and without intentional forced excitation of the structure. An additional stand-alone recording was made on bedrock to identify powerhouse harmonics.

The ambient responses were evaluated based on their spectral content with power spectral densities used to develop an understanding of where dominant behavior exists in the dam and its components. Interaction effects were identified by comparing resonances within the dam that manifested as split resonances—apparent as adjacent peaks separated by a slightly dipping plateau—which indicates tuned vibration absorption from an adjacent component.

The analysis indicates that Foster Dam is a complex system with significant interaction between the various structural subcomponents. Specifically, the tower and the piers exhibit interactions that produce regions of attenuated and shifted behaviors. This is significant because shifted and depressed responses can be expected in each region while the interaction effects persist; however, this effect may cease with the onset of damage during earthquake strong ground motion.

In general, the interaction effects will progressively increase as shaking intensity and duration increases, until the severity of earthquake-induced shaking becomes so intense that the interfaces between the various components degrade, and the components transition to behave as individual structures.

This paper is part two of a series of technical papers on ambient vibration data collection (Dupuis et al, 2025), component interactions, and LS-DYNA modeling effort (planned for USSD 2026). Part three will apply the estimated dynamic properties determined from the ambient vibration testing to validate an LS-DYNA model of Foster Dam.

ACKNOWLEDGEMENTS

The authors would like to thank the Risk Management Center of the U.S. Army Corps of Engineers for supporting this initiative and granting permission to publish this paper. The authors also wish to thank Larry Nuss and Osmar Penner for serving as external reviewers and Terry Sullivan and an additional anonymous engineer for providing invaluable insights. Thank you to the reviewers of this paper for providing suggestions which substantially improved upon its quality.

REFERENCES

Abdulamit, A., Demetriu, S., Aldea, A., Neagu, C., and Gaftoi, D. (2017). Ambient vibration tests at some buttress dams in Romania. Procedia engineering, 199, 2196-2201.

ARTeMIS Modal (2023). svibs.com/.

Calcina, S. V., Eltrudis, L., Piroddi, L., and Ranieri, G. (2014). Ambient vibration tests of an arch dam with different reservoir water levels: experimental results and comparison with finite element modelling. The Scientific World Journal, 2014.

Casiano, M.J. (2016). Extracting Damping Ratio from Dynamic Data and Numerical Solutions. Nasa, Marshall Space Flight Center, Huntsville, Alabama.

Chopra, A. K. (2020). Earthquake engineering for concrete dams: analysis, design, and evaluation. John Wiley & Sons.

Daniell, W. E., and Taylor, C. A. (1999). Effective ambient vibration testing for validating numerical models of concrete dams. Earthquake engineering & structural dynamics, 28(11), 1327-1344.

Dupuis, M., Corbett, J., Harker, J., Prusi, J., MacDougall, T., and Corbett, J. (2025). Ambient Vibrations for Model Validation of a Large Dam: Instrumentation and Testing. Proceedings of the United States Society on Dams (USSD) 2025 Annual Conference and Exhibition.

Duron, Z., Gardner, C., Gelber, M., Pham, A., ShangGuan, D., and Xia, F. (2018). Ambient Vibration Survey of Gross Dam, Final Report, submitted to AECOM, June 2018.

Duron, Z. (1996). Seven Mile Dam Vibration Testing, Results from the Second Series of Tests Performed August 14-20, 1995, submitted to BC Hydro and Power Authority, July 1996.

Hall, J. F. (1988). The dynamic and earthquake behaviour of concrete dams: review of experimental behaviour and observational evidence. Soil Dynamics and Earthquake Engineering, 7(2), 58-121.

Marple Jr, S. L. (1987). Digital spectral analysis with applications. Englewood Cliffs.

Sensequake (2023). sensequake.com/.

Smith, J. F., Ball, J. S., Novoa, N., Meremonte, M., and Levish, D. (2024). One station to rule them all: Can one seismic station forecast seismic performance of embankment dams? Proceedings of the United States Society on Dams (USSD) 2024 Annual Conference and Exhibition.